Sterics of Conserved Residue K422 in *Thermotoga maritima* Phosphoglucose Isomerase Affect Catalytic Activity

Abstract

Phosphoglucose isomerases (PGIs) are a class of enzymes that catalyze the reversible isomerization of glucose-6-phosphate (G6P) to fructose-6-phosphate (F6P) via an acid-base-catalyzed mechanism. This project was a structure-function study of the PGI from *Thermotoga maritima,* where a strictly conserved basic residue, lysine, was mutated to another basic amino acid, histidine at site 422. Previous studies suggested K422 plays a role in substrate binding. It was hypothesized that the K422H point mutation would improve the catalytic efficiency through an increase in binding affinity due to histidine's more compact structure compared to lysine. Results from kinetic assays did not align with the hypothesis, as the catalytic efficiency for K422H decreased 6-fold compared to the wild-type. Binding affinity was moderately improved, however, k_{cat} decreased significantly. Mutations at position 422 that created greater steric hindrance resulted in reduced catalytic efficiency and lower binding affinity, whereas smaller substitutions better preserved catalytic efficiency and improved binding affinity. A more comprehensive examination demonstrated that position 422 exhibits greater resilience in maintaining catalytic function compared to position 310. This understanding of K422 can be extrapolated to the understanding of other structurally conserved PGIs.

Introduction

Purpose of research

Research conducted by *Swope* et al. investigated a previously uncharacterized phosphoglucose isomerase (PGI) from *Thermotoga maritima* (TmaPGI) (PDB: 2Q8N).[1] *T. maritima* is an anaerobic and hyperthermophilic bacteria that ferments a wide range of carbohydrates, producing acetate, carbon dioxide, and hydrogen gas.[2] As seen in Figure S1, PGI functions as a catalyst for the reversible isomerization reaction between glucose-6-phosphate (G6P) and fructose-6-phosphate (F6P), a crucial step in metabolic function.[1] The PGI class of enzymes catalyzes the second step of glycolysis, the pathway for the oxidation of glucose, as well as the tenth step of gluconeogenesis, the reverse pathway for glucose synthesis. PGIs contain a central core consisting of an open twisted α/β motif, whereby a β-sheet is flanked by α-helices on either side, allowing for flexible interactions with different ligands.[3] Eukaryotic PGIs are of interest as they can function as a "moonlighting protein" and take on multiple roles; for example, many PGIs can also function as PMIs, or phosphomannose isomerase.[1]

PGIs play a major role in the prevention of lethal diseases. Molecular cloning and sequencing have been used to categorize PGIs as autocrine motility factors (AMFs). AMFs are tumor-secreted cytokines and multifunctional proteins that affect tumor growth and metastasis.[4] Tumor cells have been associated with higher rates of glycolysis and depend on increased PGI activity. Overactive AMFs are linked to aggressive cancers, such as glioblastomas and gastric and pancreatic cancers.[4] High PGI/AMF activity correlates to the prevention of apoptosis of glioblastomas, deadly central nervous system tumors, which leads to their proliferation.[5] Metastatic forms of pancreatic cancer cells are also linked to overproduction of PGIs/AMFs, especially in hypoxic environments, which heightens the motility of these cells.[6] AMFs represent possible targets for cancer therapy and may provide insight into tumor-host interactions.[4]

PGIs in *Aspergillus fumigatus,* a fatal fungal pathogen, contribute to the fungus's resistance to treatment. The F6P produced by PGI serves as a precursor for the carbohydrates in *A. fumigatus*' cell wall, contributing to its resistance against antifungal agents.[7] Analyzing the activity of PGIs can produce insights into new therapies for this fungus. *T. maritima* is a deeply branched organism; the analysis of TmaPGI may be used to gain understanding of the evolution, mechanisms, and function of PGIs derived from other bacterial, eukaryotic, and archaeal species.[1]

Previous Research on TmaPGI

Swope et al. previously determined the residues critical for TmaPGI function as well as its catalytic mechanism. TmaPGI was crystallized and cloned into the pMHI vector as a part of the Joint Center for Structural Genomics (JCSG) initiative to examine the T. *maritima* proteome.[1] *Swope* et al. explored the activity of TmaPGI and biochemically confirmed the functional mechanism. TmaPGI was identified as a phosphoglucose isomerase upon successful isomerization of F6P to G6P in a coupled enzymatic assay with glucose-6-phosphate dehydrogenase. Reaction rates followed Michaelis-Menten kinetic parameters, as seen in Table S1, and are discussed below.

Why K422H?

Previous investigations by *Swope* et al. suggest that K422 is a critical residue.[1] Figure S2b demonstrates an active site alignment between two PGIs from *T. maritima* and *Chlamydia trachomatis* (CtrPGI) (PDB: 6OTU). The active site alignment, in addition to the sequence alignment illustrated in Figure S2c, demonstrates that K422 is strictly conserved across species.[1] According to *Swope* et al., K422 and H310 facilitate the opening and closing of the sugar ring in the reversible G6P to F6P isomerization, suggesting K422 plays a key role in the catalytic activity of TmaPGI (Figure S3).[1] The kinetic analysis of H310A and K422A indicates that single mutations resulted in reduced activity, while the H310A/K422A double mutation abolishes activity even at high TmaPGI concentrations. These results suggest that H310 and K422 may compensate for each other when one is inactivated and, therefore, play a similar role during catalysis. The decrease in double mutant activity may be due to destabilization within the active site and changes in protein folding.[1]

K422H was selected as the mutation of interest to investigate the role of residue size within the active site. As shown by Figure S4, lysine has a long, flexible side chain, whereas histidine's side chain contains a shorter, more rigid imidazole ring. Substituting lysine with the more compact, yet still basic, histidine preserves the active site's overall charge environment while enabling a direct comparison of kinetic properties influenced by side-chain size. Beyond their size difference, lysine and histidine also differ in pKa, with values of 10.79 and 6.04, respectively (Figure S4). Both lysine and histidine can be classified as positively charged at pH 7, although lysine more so than histidine.

Impact of Work and Purpose

Applications of this research can be found within the characteristics of TmaPGI. TmaPGI is both a thermostable PGI and one of the most deeply branching lineages within the domain Bacteria.[1,8] A large portion of TmaPGI's genes are related to Archaea, a domain different from TmaPGI, suggesting lateral gene transfer. This could provide insight into the evolution of PGIs.[8] The thermostable classification of TmaPGI is a notable feature due to the potential industrial applications of proteins capable of tolerating high temperatures. Bioengineering uses PGI carbohydrate isomerization within industries such as wine, dairy, food/feed, and beverage production, making thermostable PGIs highly desirable for their robust and stable characteristics.[9]

This research aims to explore the structure-function relationship of TmaPGI's active site, with respect to sterics at position 422. K422 and H310 were identified as residues of interest in TmaPGI's active site. Examination of kinetic activity at positions 422 and 310 through both point and double mutations allows for further insight into how each residue and position contributes to enzyme efficiency. The impact of sterics on enzymatic activity was explored through kinetic comparisons between K422H, K422R, and K422A point mutations. By comparing kinetic data from the mutations K422H/H310A, K422A/H310K, K422A/H310A, and H310A, the resiliency of positions 422 and 310 was also investigated.

Expected effect

This work aims to determine the role of TmaPGI's active site by creating a point mutation at K422. The lysine residue will be mutated to a histidine, and the k_{cat} and K_M will be measured to determine the effect of the mutation on the catalytic efficiency of the active site. Compared to the wild-type (WT), K_M is hypothesized to decrease significantly due to the more compact size of histidine, allowing the enzyme to have a higher affinity for the substrate. Catalytic turnover, k_{cat}, is expected to moderately decrease due to evolutionary bias for the WT residue. *Swope* et al. determined that the mutated K422 resulted in a 1000x-fold increase in K_M and a 5x-fold increase in k_{cat} compared to WT, suggesting that K422 plays a greater role in substrate affinity than the rate of catalysis.[1] Therefore, k_{cat} is hypothesized to decrease on a lower order of magnitude than K_M, increasing catalytic efficiency.

Materials and Methods

Structure and multiple sequence alignments

Computational analysis was completed to explore the active site and critical residues of TmaPGI. As seen in Figure S2c, utilizing Uniprot, BLAST, and ESPript, a sequence alignment of TmaPGI and 10 other PGIs was completed to identify conserved residues, including the residue of interest K422.[10, 11, 12] Figure S2b depicts the alignment of active site residues within 5 Å of the substrate, G6P, in TmaPGI and CtrPGI. CtrPGI was chosen for the presence of a crystallised substrate, linear glucose-6-phosphate (G6P).

For the cyclic WT and mutant, K422H was introduced to TmaPGI in Chimera.[13] Docking was performed with SwissDock.[14] Docking orientations underwent optimization starting with a comparison to the phosphate group of linear G6P of CtrPGI in Chimera.[13] Orientations were then considered based on the critical residues (H310, K422, E281) mentioned in the proposed cis-endol mechanism in Figure S3.[1] The bond length between the three critical residues and the site of interaction with G6P was optimized alongside sP-dG values. The orientation with the lowest optimized bond lengths and sP-dG was chosen (Table S2, Table S3). Hydrogen bonds were then determined for the WT TmaPGI and K422H mutant active sites (Figure S5).

Mutagenesis

The transformation of the pMHI vector encoding TmaPGI into HK100 *Escherichia coli* cells was performed by the JCSG. The pMHI vector conferred ampicillin resistance and an amino-terminal 6xHis tag. To generate the K422H mutation, PCR using the Polymerase Incomplete Primer Extension (PIPE) was performed with a BioRad C1000 Thermocycler.[15] SDS-PAGE was used to monitor successful amplification during the PCR reaction. After PIPE-PCR, HK100 competent *E. coli* cells were transformed with the mutagenized plasmid. The plasmid DNA was purified using a QiaPrep Spin Miniprep Kit (Qiagen). The mutation was confirmed by Sanger sequencing (GENEWIZ) with a pBAD backward primer.[16] The DNA sequence was translated to a protein sequence via Expasy to confirm mutation presence.

Expression of recombinant proteins and purification

A small-scale starter culture was created 24 hours before the experiment start time. All work was performed no more than 30 cm from a lit Bunsen burner in a sterile worksite. In a 15 mL culture tube, 7 mL of LB-Amp media (provided at 25 g/L of dry LB media, 1 mL of 100 mg/L Amp) was aliquoted. Subsequently, a colony of *E. coli* cells containing a pMH1 vector obtained from

JCSG with either the TmaPGI WT or K422H mutant was transferred utilizing an applicator stick. The starter was placed in a shaking incubator at 250 rpm at 37°C.

The following morning, a small-scale starter was inoculated into a 1 L culture at a sterile work surface. 1 mL of ampicillin (100 mg/mL) was added to a previously autoclaved 1 L of LB in a 2 L culture flask. The remaining overnight cultures of the TmaPGI WT and K422H were distributed into their respective flasks and placed in an incubator shaker at 250 rpm at 37°C. Induction of expression was completed 4 hours post-inoculation by adding 1 mL of arabinose (provided 20%, 0.02% final) to each flask. The flasks were left to shake at 250 rpm at 37°C, allowing for protein expression to be induced once the OD_{600} reached 0.6.

Cells were harvested by centrifugation at 10,000 x g for five minutes. For lysis, cells were resuspended in complete lysis buffer (50 mM Tris pH 8, 150 mM NaCl, 2 mM $MgCl_2$, 0.25 mg/mL lysozyme, and 0.04 µL/mL DNase). The cells in complete lysis buffer were incubated at room temperature for 15 minutes before storing at -20 ºC. A freeze-thaw cycle was performed to ensure complete lysis. Expression of recombinant proteins was monitored by SDS-PAGE analysis.

Affinity Chromatography and SDS-PAGE

Preparation of cell lysate for immobilized metal affinity chromatography (IMAC) began with thawing and centrifugation at 5,100 rpm for 30 minutes. IMAC occurred in a Bio-Rad chromatography column. A run-through was completed with dH_2O followed by the addition of 2 mL of 50% slurry of HiBond™ Ni-NTA Agarose resin. The column volume (CV) was 1 mL. The resin was washed with 30 CV of dH_2O and equilibrated by passing 10 CV of lysis buffer (50 mM Tris pH 8, 150 mM NaCl, and 2 mM $MgCl_2$) through the column. The cell lysate was added to the column, and the flow-through was collected and saved. Non-specifically bound protein was washed from the resin by flowing 15 CV of wash buffer (50 mM Tris pH 8, 150 mM NaCl, and 10 mM imidazole) through the column. Protein bound to the resin was eluted with 10 CV of elution buffer (50 mM Tris pH 8, 150 mM NaCl, and 400 mM imidazole). Both the wash and elution fractions were collected by stepwise elution in two fractions, and a sample from the resin was collected from the column and combined with 30 µL of diluted loading buffer (10 µL 4x SDS-SLB (0.5M Tris-Cl pH 6.8, 0.278M SDS, 40% (v/v) Glycerol, 5% (v/v) BME, 597 µM bromophenol blue) and 20 µL dH_2O).

To monitor purification, SDS-PAGE was run using 30 µL aliquots from each collected sample with 10 µL of 4x SDS SLB combined in each sample (a 3:1 ratio). Samples were prepared by vortexing and heating on heat blocks set to 80°C for a minimum of 5 minutes. A Mini- PROTEAN TGX Stain - Free Gel (4-15%) was loaded with 15 µL of each sample. 10 µL of Bio-Rad Precision Plus ProteinTM Unstained Standard was loaded into a well as a reference and run at 300 volts for 18 min. The gel was then visualized using the stain-free tray for a Gel Doc EZ Imager. Using the ProtParam tool by Expasy, the molecular weight of TmaPGI was determined to be 51,947 Da. Bands were examined around the 50 kDa mark to confirm the successful expression of the TmaPGI protein in both the WT and mutant samples.

Dialysis and Quantification

The purified protein from the elution fractions was dialyzed three times at room temperature for at least two hours against 500 mL of dialysis buffer each (50 mM Tris base, pH 7, and 150 mM NaCl). Dialysis was performed as a method of buffer exchange. The chosen dialysis buffer was used for removing small molecules, such as imidazole, while maintaining conditions where the protein remains dissolved. Dialysis was performed using a 3.5K MWCO snakeskin dialysis tubing. The overall dilution obtained was 1:125,000. The concentration of TmaPGI protein was determined using a NanoDrop spectrophotometer at 280 nm. Sample volumes were 2 µL, and the blank was run with ultra-pure water. The extinction coefficient for TmaPGI was calculated to be 54,320 $M^{-1}cm^{-1}$. The readings in mg/mL were converted to molar concentration using the predicted molecular weight of TmaPGI, 51.94 kDa.

Kinetic assay using coupled Glucose-6-phosphate dehydrogenase

The catalytic activity of TmaPGI was determined spectrophotometrically by NADPH absorbance at 340 nm using an Epoch 2 microplate reader (Biotek). The coupled enzyme assay to measure TmaPGI activity was adapted from *Swope* et al.[1] The ideal protein concentration for the kinetic assays was determined by constructing a progress curve. The progress curve assay was performed in Buffer A (50 mM Tris pH 7, 150 mM NaCl) at 21°C in reactions containing 20 mM F6P, 0.6 U/mL G6PDH, 1 mM $NADP^+$, and 10 mM $MgCl_2$ with varying TmaPGI concentrations (0.5 µM- 2 µM, dilution factor of 2). Negative controls were run in Buffer A with 20 mM F6P, 0.6 U/mL G6PDH, 1 mM $NADP^+$, and 10 mM $MgCl_2$. A protein concentration of 1 µM gave the most linear change in absorbance with saturating F6P concentrations for both mutant and WT TmaPGI.

Kinetic assays were performed in Buffer A at 21°C in reactions containing 1 μM TmaPGI, 0.6 U/mL G6PDH, 1 mM $NADP^+$, and 10 mM $MgCl_2$ with varying F6P concentrations (0.0024 mM- 40 mM, dilution factor of 2). Negative controls were run in Buffer A with 40 mM F6P, 0.6 U/mL G6PDH, 1 mM $NADP^+$, and 10 mM $MgCl_2$. Coupled assay reactions were carried out in 96-well plates using 200 μL reaction volumes. Each F6P concentration was run in triplicate, with TmaPGI added last, immediately before absorbance measurements. Absorbance readings were recorded at 15-second intervals for 30 minutes. The rate of the reaction was determined by dividing the change in absorbance by the extinction coefficient of NADPH (6220 M^{-1} cm^{-1}) and the path length (0.5 cm). Background rates were subtracted from calculated rates. Kinetic parameters were generated based on the initial rate of NADPH formation versus F6P concentration and fit with the Hill equation in SciDAVis.

Results

Sequence Alignments, Purification, and Quantification

A multiple sequence alignment of the active site of TmaPGI with ten other known PGIs confirmed the conservation of K422 across species, as shown in Figure S2c. To continue the exploration, the protein was mutated using PIPE mutagenesis, transformed, and expressed. SDS-PAGE was used to monitor purification throughout IMAC, with clear bands at ~50 kDa observed in both the cell lysis and elution fractions, confirming expression and purification (Figure S6). As shown in Figure S6a, the WT protein displays additional bands in the elution fractions outside of the expected ~50 kDa range, indicating lower purity. In contrast, Figure S6b shows fewer extraneous bands in the elution columns for the K422H mutant, suggesting a higher level of purity compared to the WT. Following dialysis, the concentrations of WT and K422H mutant proteins were determined using a NanoDrop spectrophotometer, yielding values of 8.77 μM and 5.68 μM, respectively.

Kinetic Assays

A progress curve assay was performed to determine the optimal concentration of WT and K422H TmaPGI for use in kinetic assays. A concentration of 1 μM resulted in the fastest rate with the most linear change in absorbance in saturated F6P concentrations. A coupled enzymatic assay with G6PDH was conducted to assess the rate of WT and K422H activity across varying concentrations of F6P, as shown in Figure 1.

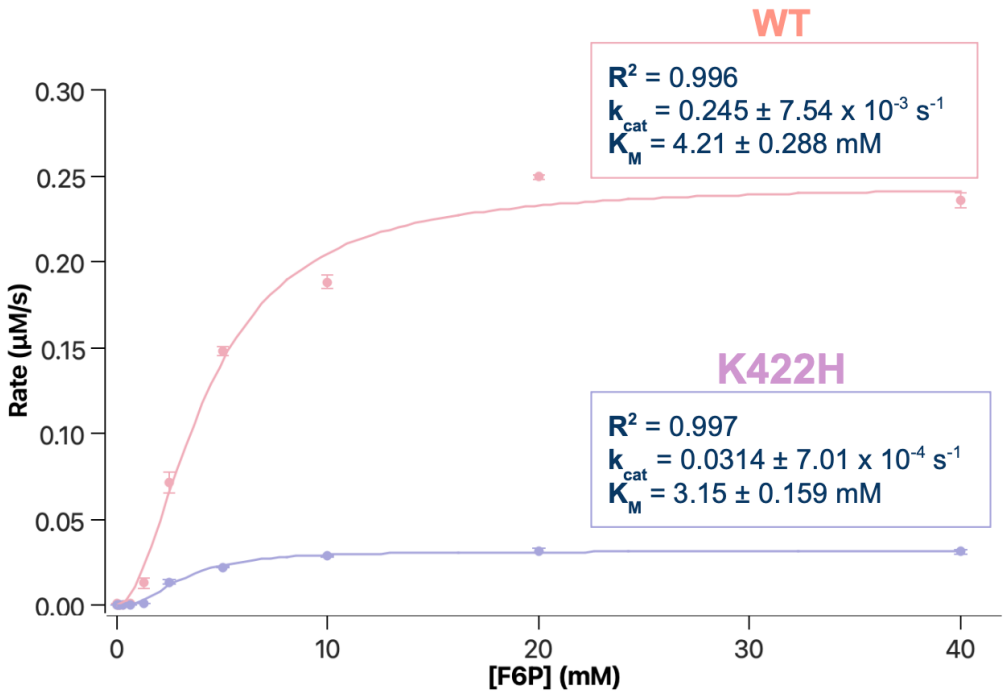

Figure 1. Rates of K422 & K422H activity versus fructose-6-phosphate concentration fit to the Hill equation. The optimal concentration of both WT and mutant TmaPGI was determined to be 1 µM. Samples were run in triplicate with 0.6 U/mL G6DPH, 1 mM $NADP^+$, 10 mM $MgCl_2$, 1 µM TmaPGI, and varying F6P concentrations (0.0024 - 40 mM) in 150 mM NaCl, 50 mM Tris, pH 7. Absorbance at 340 nm was read every 15 s for 30 min. K_M for WT (4.21 ± 0.29 mM) and K422H (3.15 ± 0.16 mM,) along with the k_{cat} for WT (0.245 ± 0.008 s^{-1}) and mutant (0.0314 ± 0.0007 s^{-1}), were determined from fitting the data in SciDAVis to the Hill equation. The R^2 was 0.996 for WT and 0.997 for K422H. Error bars represent one standard deviation.

In Figure 1, the data points represent the average rate of three trials conducted across F6P concentrations ranging from 0.0024 mM to 40 mM, using twofold serial dilutions. The data was fit to the Hill equation, resulting in R^2 values of 0.996 and 0.997 for WT and K422H, respectively. K_M and k_{cat} were determined to be 4.21 $\pm$ 0.288 mM and 0.245 $\pm$ 0.00754 s^{-1}, respectively, for WT and 3.15 $\pm$ 0.159 mM and 0.0314 $\pm$ 0.000701 s^{-1}, respectively, for K422H. Both data sets exhibited positive cooperativity, with WT displaying a Hill coefficient (n) of 1.90 ± 0.199 and K422H showing an n value of 2.30 ± 0.225. In comparison to WT, K422H retained 17.1% catalytic efficiency.

Comparisons with other K422 point mutations

Table 1. Kinetic parameters of TmaPGI variants with fructose-6-phosphate (G6PDH-Couple Assay) from WT and K422 Mutants K422H, K422R, and K422A.[a]

TmaPGI Variant	K_M	k_{cat}	Catalytic Efficiency[b]
WT	100%	100%	100%
K422H	74.8%	12.8%	17.1%
K422R	107%	12.0%	11.3%
K422A[c]	12.9%	5.64%	43.5%

[a]Kinetic data from K422R and K422A were obtained from separate studies conducted by other groups in the same lab; parameters for K422R and K422A were reported in relative change to their collected WT data. For K422R and K422A WT and mutant data, see Table S4. **Red** indicates unfavorable changes. **Green** indicates favorable changes.
[b]Catalytic efficiency is relative to each mutant's respective wild-type and calculated as k_{cat}/K_M.
[c]Kinetic data for K422A was obtained from the group performing the K422A/H310R double mutation.

A comparison of three related K422 point mutations are reported in Table 1. The kinetic parameter values from which the comparison percentages were derived are listed in Table S4. The K_M for the K422H mutation was 74.8% of the WT. K422R had a K_M increase of 7% while K422A had a K_M decrease, with 12.9% retained relative to their respective WT values. All k_{cat} values experienced a decrease, with 12.8%, 12.0%, and 5.64% retained compared to WT for K422H, K422R, and K422A, respectively. After normalizing the WT catalytic efficiency (k_{cat}/K_M) to 100%, the catalytic efficiencies for the mutant TmaPGIs were: 17.1% for K422H, 11.3% for K422R, and 43.5% for K422A.

Discussion

Why Hill's Equation?

When analyzing the WT and K422H mutant data in SciDAVis using the Michaelis-Menten equation, the resulting K_M values showed significant discrepancies and larger errors compared to those obtained using the Hill equation. The Michaelis-Menten fit yielded a K_M of 7.02 ± 1.57 mM for the WT, whereas the Hill fit produced a more consistent value of 4.21 ± 0.288 mM. Similarly, for the K422H mutant, the Michaelis-Menten model gave a K_M of 5.02 ± 1.33 mM, compared to 3.15 ± 0.159 mM from the Hill equation. The substantially higher standard deviations in the Michaelis-Menten fits suggest poor model accuracy and reduced reliability in estimating kinetic parameters. Therefore, the Hill equation was chosen to provide a more precise and appropriate model for fitting the data.

Kinetic results did not support initial predictions

K422H was hypothesized to increase the catalytic efficiency of TmaPGI compared to WT. The K_M for K422H was predicted to decrease significantly compared to WT due to histidine having a more compact structure compared to lysine, thus contributing to a higher binding affinity. k_{cat} was projected to moderately decrease due to evolutionary bias for the WT residue. Previous data from *Swope* et al. suggested that K422 played a greater role in substrate affinity than enzyme catalysis.[1] Therefore, the decrease in K_M was hypothesized to be on a lower order of magnitude than the decrease in k_{cat}, resulting in an overall increase in enzymatic efficiency for mutated TmaPGI.

As hypothesized, the K_M for K422 decreased significantly from 4.21 mM to 3.15 mM for K422H, indicating an increased binding affinity compared to WT. The k_{cat}, however, decreased significantly from 0.245 s^{-1} to 0.0314 s^{-1} for K422H, suggesting reduced catalytic efficiency compared to WT. K422H retained only 17.1% of the original catalytic efficiency. The negative effect of histidine on catalytic efficiency may be explained by an alteration in active site orientation. As shown by Figure S5, K422, H310, and E281 in the WT contained one hydrogen bond each with G6P in the active site. Once mutated, K422H no longer hydrogen bonded with the substrate, and E281 possessed an additional hydrogen bond to G6P. As previously mentioned, K422 and H310 facilitate the opening and closing of the sugar ring while E281 catalyzes the reversible isomerization of G6P to F6P.[1] This loss of hydrogen bonding in K422H and additional hydrogen bond in E281 may have disrupted this mechanism, ultimately impairing the isomerization process and reducing catalytic efficiency.

Comparisons reveal impact of sterics

Position 422 is influenced by the steric "bulk" of the residue present. As seen in Table 1, the bulkiest basic amino acid, arginine, led to the greatest decrease in catalytic efficiency (11.3% retained compared to WT), followed by histidine (17.1% retained) and then alanine (43.5% retained). Therefore, an increase in side-chain bulk at position 422 is associated with reduced catalytic efficiency. Additionally, the binding affinity, K_M, improved for less bulky residues; the bulkiest amino acid, arginine, resulted in a 107% increase in $K_{M,}$ while alanine, the least bulky residue, improved binding affinity through an observed 12.9% K_M compared to its WT. Bulkier side chains can hinder proper G6P positioning in the active site, as demonstrated by the bulkiest

residue, arginine, with the worst binding affinity, and the least bulky residue, alanine, with the best binding affinity.

Future work

Table 2. Kinetic parameters[a] of K422H/H310A and K422A/H310A Mutations.[b]

TmaPGI Variant	K_M	k_{cat}	Catalytic Efficiency
K422H/H310A	48.5%	1.77%	3.66%
K422A/H310K	150%	7.39%	1.99%
K422A/H310A[c]	NA	NA	NA
H310A[d]	75,161%	373.56%	0.50%

[a]**Red** indicates unfavorable changes. **Green** indicates favorable changes.
[b]Kinetic data from K422H/H310A and K422A/H310A were reported in relative change to their collected WT data.
[c]K422A/H310A kinetic data was obtained from reference 1. NA indicates no activity.
[d]H310A kinetic data was obtained from reference 1.

Swope et al. found that K422 and H310 may functionally compensate for each other if either residue is impaired. Further insight into this relationship can be explored through the double mutations K422A/H310K and K422H/H310A. Comparison of kinetic parameters, as seen in Table 2, shows that the double mutant K422A/H310K leads to an increase in K_M and a decrease in k_{cat} and catalytic efficiency. K422H/H310A similarly leads to a decrease in k_{cat} and catalytic efficiency, however, K_M also decreases. K422A/H310K and K422H/H310A both experience an extreme decrease in catalytic efficiency (1.99% and 3.66% retained compared to WT, respectively). The K422H, K422R, and K422A mutants, as previously described, maintained catalytic efficiency within the range of 11.30% to 43.5%, higher percentages than those of the double mutants. This implies that position 422 is more resilient to mutations than position 310. This is further supported by the H310A mutation, which decreased catalytic efficiency to 0.50% of WT, compared to K422A with 43.5% of WT efficiency. To further explore the adaptability at these two positions, the double mutation, K422H/H310K, is proposed (Figure S7). This mutation will cause steric changes within the active site while maintaining the basicity at both positions by allowing both lysine and histidine to remain. Ultimately, this mutation will determine the structural flexibility of the active site and the degree of residue specificity required by TmaPGI to sustain catalytic efficiency.

Conclusions

Position 422, a highly conserved and functionally essential residue in TmaPGI, is sensitive to steric effects yet demonstrates greater resilience to active site modifications than position 310.

Analysis of point mutations at K422 revealed that introducing greater steric hindrance reduced catalytic efficiency and increased K_M, whereas smaller substitutions better preserved catalytic efficiency and decreased K_M. Examining position 422 in a wider context through the double mutations K422H/H310A, K422A/H310K, and K422A/H310A, along with H310A, demonstrates that position 422 exhibits greater resilience in maintaining catalytic function compared to position 310. Future research through the study of the K422H/H310K double mutation may provide further knowledge into the resiliency of each position. The insights gained from this study into the role and functional flexibility of residue 422 contribute to a deeper understanding of the TmaPGI active site. This knowledge is particularly valuable in the medical and industrial fields, as PGIs represent potential targets for the treatment of serious diseases and may be used for their robust and stable characteristics across a multitude of industries.

Acknowledgements

This research was made possible by the University of Virginia Department of Chemistry and the Biological Chemistry II Lab Course, CHEM 4421. A special thanks to the queen *Dr. Price*, and our TA, *Andrew Spira*, for their guidance and support in this research.

References

1. Swope, N.; Lake, K. E.; Barrow, G. H.; Yu, D.; Fox, D. A.; Columbus, L. TM1385 from *Thermotoga Maritima* Functions as a Phosphoglucose Isomerase via Cis-Enediol-Based Mechanism with Active Site Redundancy. *Biochimica et Biophysica Acta (BBA) - Proteins and Proteomics* **2021**, *1869* (4), 140602. https://doi.org/10.1016/j.bbapap.2021.140602.
2. Schut, G. J.; Adams, M. W. W. The Iron-Hydrogenase of Thermotoga Maritima Utilizes Ferredoxin and NADH Synergistically: A New Perspective on Anaerobic Hydrogen Production. *Journal of Bacteriology. **2009**, 4451–4457.* https://doi.org/10.1128/jb.01582-08.
3. Sun, Y.-J.; Chou, C.-C.; HsIAO, C.-D. The Crystal Structure of a Multifunctional Protein: Phosphoglucose Isomerase/Autocrine Motility Factor/Neuroleukin. *Proc. Natl. Acad. Sci.* **1999**, *96* (10), 5412-5417. https://doi.org/10.1073/pnas.96.10.5412.
4. Ma, Y.-T.; Xing, X.-F.; Dong, B.; Cheng, X.-J.; Guo, T.; Du, H.; Wen, X.-Z.; Ji, J.-F. Higher Autocrine Motility Factor/Glucose-6-Phosphate Isomerase Expression Is Associated with Tumorigenesis and Poorer Prognosis in Gastric Cancer. *Cancer Manag Res* **2018**, *10*, 4969–4980. https://doi.org/10.2147/CMAR.S177441.

5. Li, Y.; Wei, Z.; Dong, B.; Lian, Z.; Xu, Y. Silencing of Phosphoglucose Isomerase/Autocrine Motility Factor Decreases U87 Human Glioblastoma Cell Migration. Int J Mol Med **2016**, 37 (4), 998–1004. https://doi.org/10.3892/ijmm.2016.2500.
6. Funasaka, T.; Yanagawa, T.; Hogan, V.; Raz, A. Regulation of Phosphoglucose Isomerase/Autocrine Motility Factor Expression by Hypoxia. *FASEB J* **2005**, *19* (11), 1422–1430. https://doi.org/10.1096/fj.05-3699com.
7. Zhou, Y.; Yan, K.; Qin, Q.; Raimi, O. G.; Du, C.; Wang, B.; Ahamefule, C. S.; Kowalski, B.; Jin, C.; van Aalten, D. M. F.; Fang, W. Phosphoglucose Isomerase Is Important for Aspergillus Fumigatus Cell Wall Biogenesis. *mBio* **2022**, *13* (4), e0142622. https://doi.org/10.1128/mbio.01426-22.
8. Logsdon, J. M.; Faguy, D. M. Evolutionary Genomics: Thermotoga Heats up Lateral Gene Transfer. *Current Biology* **1999**, *9* (19), R747–R751. https://doi.org/10.1016/S0960-9822(99)80474-6
9. Maqsood, A.; Shakir, N. A.; Aslam, M.; Rahman, M.; Rashid, N. Structural and Functional Investigations of Pcal_0606, a Bifunctional Phosphoglucose/Phosphomannose Isomerase from Pyrobaculum Calidifontis. *Int J Biol Macromol* **2024**, *279* (Pt 1), 135127. https://doi.org/10.1016/j.ijbiomac.2024.135127.
10. Altschul, S. F.; Madden, T. L.; Schäffer, A. A.; Zhang, J.; Zhang, Z.; Miller, W.; Lipman, D. J. Gapped BLAST and PSI-BLAST: A New Generation of Protein Database Search Programs. *Nucleic Acids Res* **1997**, *25* (17), 3389–3402. https://doi.org/10.1093/nar/25.17.3389.
11. UniProt Consortium. UniProt: The Universal Protein Knowledgebase in 2023. *Nucleic Acids Res* **2023**, *51* (D1), D523–D531. https://doi.org/10.1093/nar/gkac1052.
12. Robert, X.; Gouet, P. Deciphering Key Features in Protein Structures with the New ENDscript Server. *Nucleic Acids Res* **2014**, *42* (Web Server issue), W320-324. https://doi.org/10.1093/nar/gku316.
13. Pettersen, E. F.; Goddard, T. D.; Huang, C. C.; Couch, G. S.; Greenblatt, D. M.; Meng, E. C.; Ferrin, T. E. UCSF Chimera--a Visualization System for Exploratory Research and Analysis. J Comput Chem **2004**, 25 (13), 1605–1612. https://doi.org/10.1002/jcc.20084.
14. Bugnon, M.; Röhrig, U. F.; Goullieux, M.; Perez, M. A. S.; Daina, A.; Michielin, O.; Zoete, V. SwissDock 2024: Major Enhancements for Small-Molecule Docking with Attracting Cavities and AutoDock Vina. *Nucleic Acids Research* **2024**, *52* (W1), W324–W332. https://doi.org/10.1093/nar/gkae300.

15. Klock, H. E.; Lesley, S. A. The Polymerase Incomplete Primer Extension (PIPE) Method Applied to High-Throughput Cloning and Site-Directed Mutagenesis. *Methods Mol Biol* **2009**, *498*, 91–103. https://doi.org/10.1007/978-1-59745-196-3_6.
16. Sanger, F.; Nicklen, S.; Coulson, A. R. DNA Sequencing with Chain-Terminating Inhibitors. *Proc Natl Acad Sci U S A* **1977**, *74* (12), 5463–5467. https://doi.org/10.1073/pnas.74.12.5463.

Supplementary Information

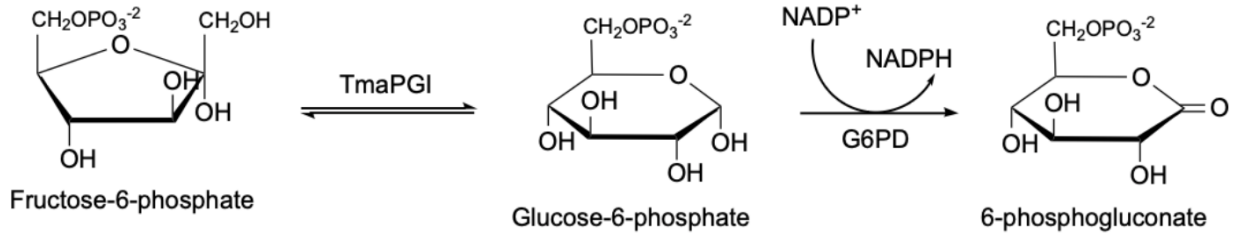

Figure S1. TmaPGI and G6PD coupled assay reaction. The figure demonstrates the reversible isomerization of fructose-6-phosphate to glucose-6-phosphate through phosphoglucoisomerase (TmaPGI). This reaction is followed by glucose-6-phosphate dehydrogenase (G6PD), which produces NADPH. The reduction of $NADP^+$ with G6PD is measured through the absorbance of NADPH at 340 nm. Individual hydrogens are not displayed.

Table S1. Michaelis-Menten kinetic parameters of TmaPGI WT and K422A with fructose-6-phosphate (G6PDH-Couple Assay). Adapted from reference 1.

TmaPGI Variant	K_M (mM)	k_{cat} (s^{-1})	k_{cat}/K_M (mM^{-1} s^{-1})
WT	0.31 ± 0.03	17.4 ± 0.4	58.8 ± 6.2
K422A	478 ± 180	86 ± 13	0.2 ± 0.1

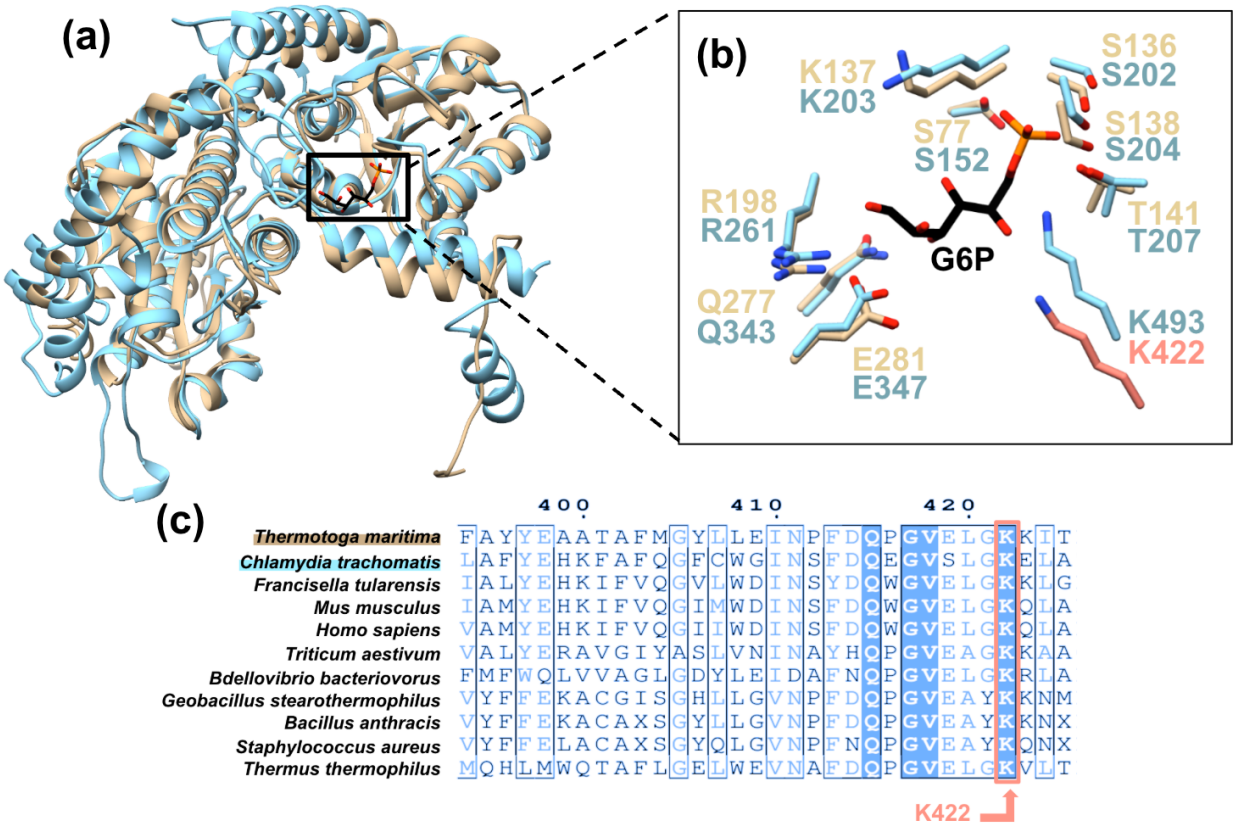

Figure S2. **Structure, active site, and sequence alignment of PGIs.** Conservation of K422 is demonstrated through (a) Features structure alignment between *Thermotaga maritima* phosphoglucoisomerase (TmaPGI (PBD: 2Q8N)) and *Chlamydia trachomatis* phosphoglucoisomerase (CtrPGI (PBD: 6OTU)) crystalized with glucose-6-phosphate (G6P) substrate. The RMSD for the aligned TmaPGI and CtrPGI was 1.001 Å, which implies similarity (b) Features active site alignment between TmaPGI and CtrPGI crystalised with glucose-6-phosphate (G6P) substrate. Alignments were completed utilizing Chimera. (c) Espript generated a partial multiple sequence alignment with TmaPGI and 10 homologous PGIs, including CtrPGI. The salmon box highlights the highly conserved K422.

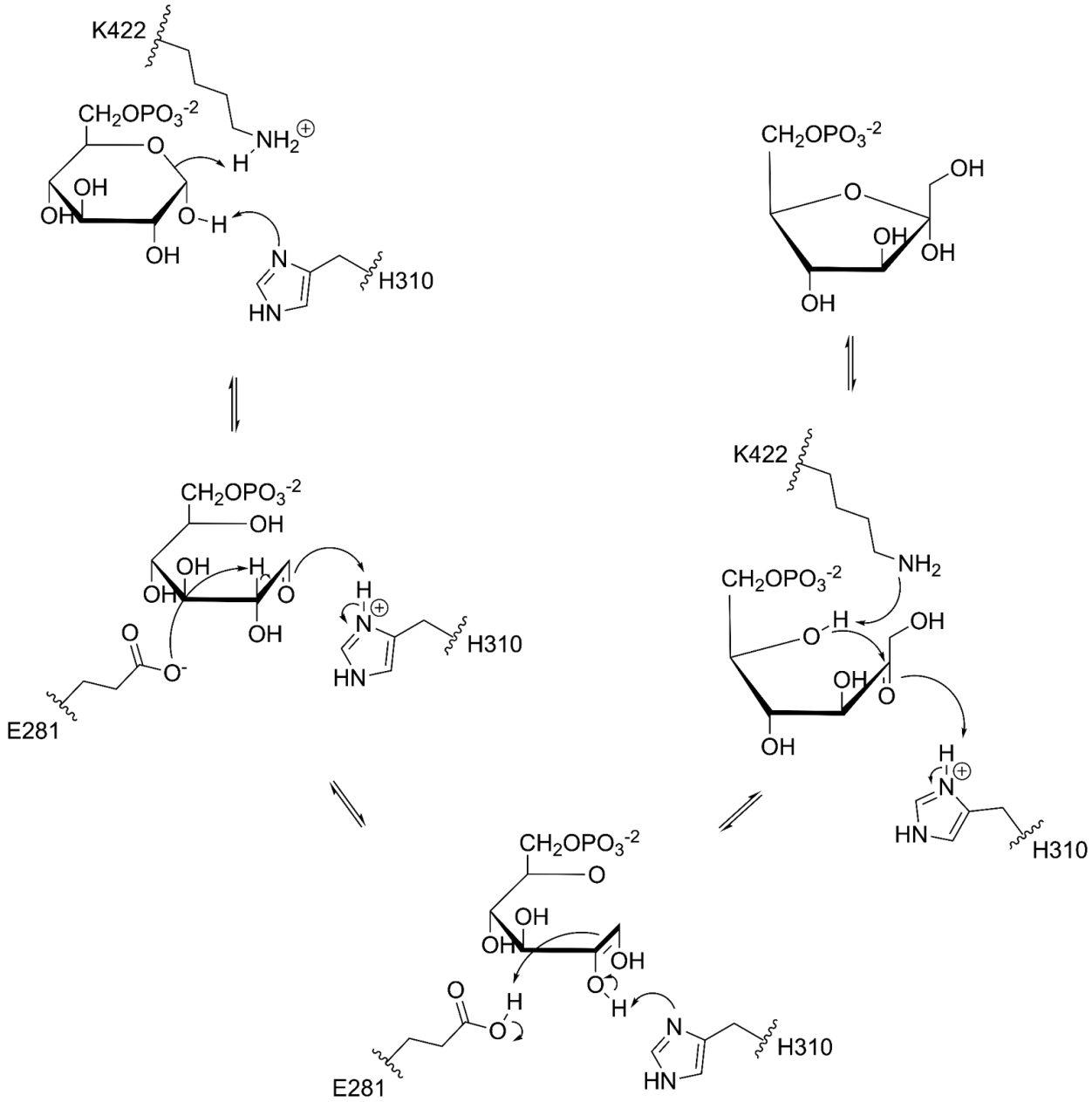

Figure S3. Cis-endol mechanism converting G6P to F6P. TmaPGI proton exchange is aided by active site residues, whereby H310 initiates the G6P ring opening by accepting a proton from the alcohol at C1 and K422 donates a proton to the sugar ring, forming a hydroxyl at C5. E281 extracts a proton from C2, forming the cis-enediol intermediate with H310 accepting the leaving proton. E281 donates the proton back to C1, completing isomerization to linear F6P. Finally, H310 donates a proton to the carbonyl at C2 and K422 accepts a proton from the oxygen atom in the sugar ring, returning the substrate to its cyclic form. Mechanism adapted from reference 1.

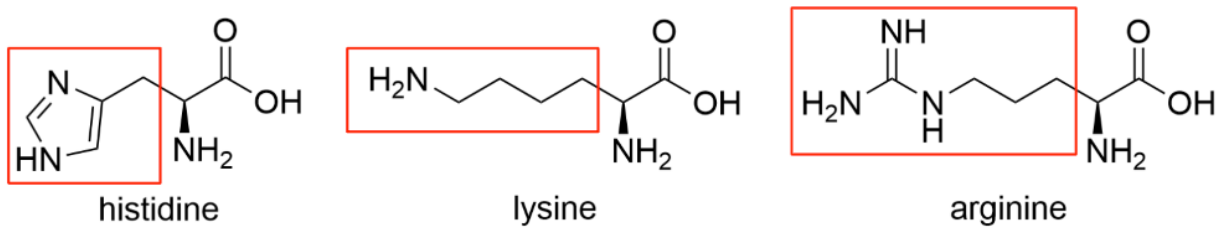

Figure S4. Structures of basic amino acids. From left to right, the basic amino acids histidine, lysine, and arginine are shown, which have pK_a values of 6.04, 10.79, and 12.48, respectively. The side chain of each amino acid is outlined in red.

Table S2. Bond lengths (BL), Gibbs free energy, and optimized score[a] of top 17 cyclic-G6P docked poses of wild-type TmaPGI.

Pose	BL 1 (Å)	BL 2 (Å)	BL 3 (Å)	sP-dG	Optimized Score
48	3.145	6.898	2.850	-6.8641	8.000
49	2.600	3.005	2.349	-6.7754	5.000
50	**3.767**	**2.480**	**2.286**	**-6.8101**	**3.500**
53	3.230	5.107	4.862	-6.5743	10.75
55	3.148	2.846	2.431	-6.5928	6.000
120	6.323	6.150	3.229	-6.3951	14.00
142	2.874	2.586	2.321	-6.4756	4.500
143	4.413	2.695	2.774	-6.5599	9.250
144	4.409	2.699	2.762	-6.5657	8.750
145	4.296	2.588	2.638	-6.1913	9.500
149	4.058	2.267	2.618	-6.2425	7.250
201	4.604	2.854	3.147	-6.2616	12.50
202	4.195	2.100	3.517	-6.1314	10.25
203	4.106	2.887	2.887	-6.507	10.50
204	4.233	2.240	3.248	-6.1372	10.25
205	4.466	2.899	3.914	-6.0496	14.75
206	3.141	2.834	2.400	-6.0416	8.250

[a]Optimized scores were determined by sorting categories, with their pose number, by most desirable outcomes (lowest number to highest). Outputs were then ranked (lowest, most ideal value=1). Each pose was assigned an unweighted average to equally weight each input category, with the lowest value being most ideal. WT pose orientation chosen is represented in salmon.

Table S3. Bond lengths (BL), Gibbs free energy, and optimized score[a] of top 24 cyclic-G6P docked poses of K422H TmaPGI.

Pose	BL 1 (Å)	BL 2 (Å)	BL 3 (Å)	sP-dG	Optimized Score
41	6.031	3.253	2.926	-6.4226	13.25
42	5.557	4.821	3.852	-6.7205	13.75
76	**4.583**	**4.068**	**3.668**	**-7.0151**	**7.500**
77	4.974	5.302	5.227	-6.8703	13.75
78	5.087	5.375	5.204	-6.6333	16.75
79	4.949	5.327	5.208	-6.6923	15.50
80	5.310	5.215	4.138	-6.7655	14.25
81	6.371	5.455	4.011	-6.8340	13.50
82	4.482	4.174	2.629	-6.6446	8.000
83	5.240	3.533	3.077	-6.6705	10.50
88	5.732	4.301	3.295	-6.5284	13.50
89	6.545	5.097	3.529	-7.0235	13.00
91	6.020	4.795	4.031	-6.4147	17.25
121	4.102	1.993	4.861	-6.0575	11.50
122	3.015	2.871	6.064	-6.1099	13.00
154	4.935	6.024	7.729	-6.4436	19.00
158	6.038	2.850	2.850	-6.8335	8.500
159	6.172	3.092	2.765	-6.8037	9.500
160	6.172	3.097	2.759	-6.8045	9.500
161	5.248	1.911	3.527	-6.7343	8.000
162	4.604	3.394	3.679	-6.5088	11.25
163	4.389	2.208	4.496	-6.3524	11.50
193	3.770	4.394	6.701	-6.5805	13.75
243	4.866	1.997	5.200	-6.5035	11.75

[a]Optimized scores were determined by sorting categories, with their pose number, by most desirable outcomes (lowest number to highest). Outputs were then ranked (lowest, most ideal value=1). Each pose was assigned an unweighted average to equally weight each input category, with the lowest value being most ideal. K422H pose orientation chosen is represented in plum.

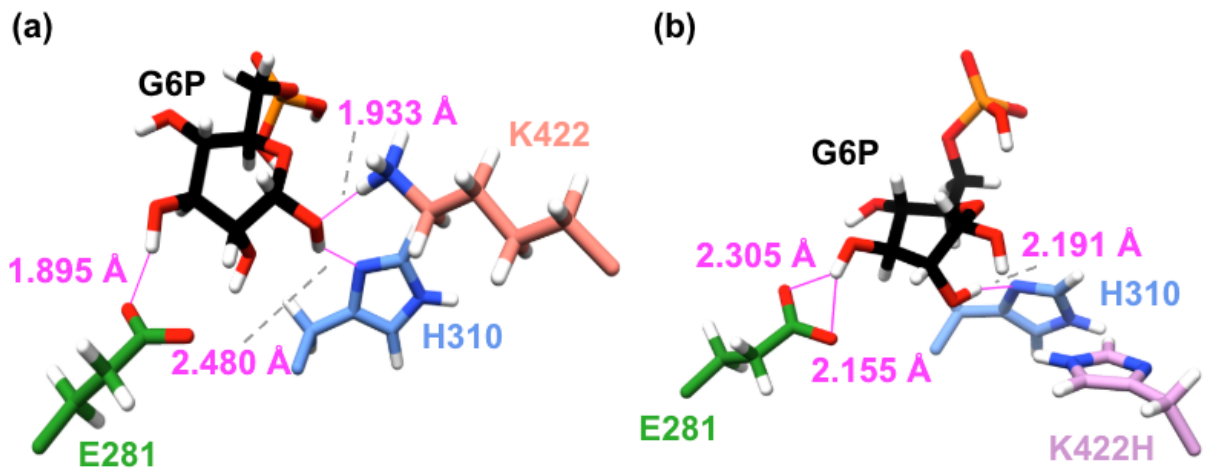

Figure S5. Docked G6P in the active site to determine H-bonds. Active site of the WT and K422H mutant (a) shows the calculated H-bond between K422, H310, and E281 and G6P at 1.933 Å, 2.480 Å, and 1.895 Å, respectively. The H-bonds are represented by a pink line. (b) Shows the calculated H-bond between K422H, H310 (2.191 Å), and E281 (2.155 Å and 2.305 Å). The H-bonds are represented by a pink line.

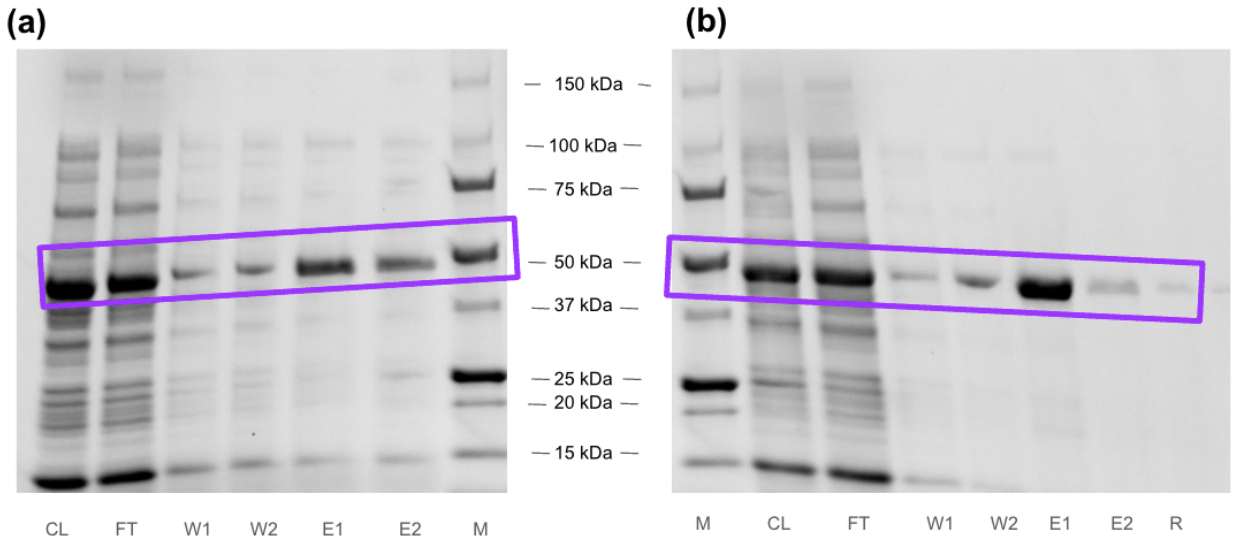

Figure S6. SDS-PAGE monitoring induction and purification processes. (a) This figure represents the SDS-PAGE gel that was run with varying fractions taken throughout the affinity chromatography procedure for the wild-type. The rightmost column features the standard to the Bio-Rad Precision Plus Protein Unstained Standard, followed by the elution 2 (E2), elution 1 (E1), wash 2 (W2), wash 1 (W1), flow-through (FT), and lysate columns, respectively. The purple block represents the expected TmaPGI protein at ~51 kDa. (b) This figure represents the SDS-PAGE gel that was run with varying fractions taken throughout the affinity chromatography procedure for K422H. The leftmost column features the standard to the Bio-Rad Precision Plus Protein Unstained Standard, followed by the lysate column (CL), flow-through (FT), wash 1 (W1), wash 2 (W2), elution 1 (E1), elution 2 (E2), respectively. The purple block represents the expected TmaPGI K422H mutantat ~51 kDa.

Table S4. Kinetic parameters of TmaPGI variants with fructose-6-phosphate (G6PDH-Couple Assay) for WT and Mutants for K422H, K422R and K422A.

Group Name	TmaPGI Variant	K_M (mM)	k_{cat} (s^{-1})	k_{cat}/K_M (mM^{-1} s^{-1})
K422H	WT	4.21 ± 0.29	0.245 ± 0.008	0.0582 ± 0.00437
	K422H	3.15 ± 0.16	0.0314 ± 0.0007	0.00997 ± 0.00055
K422R	WT	0.552 ± 0.079	1.48 ± 0.05	2.68 ± 0.39
	K422R	0.588 ± 0.042	0.178 ± 0.003	0.303 ± 0.022
K422A/ H310R	WT	0.650 ± 0.230	0.550 ± 0.090	0.850 ± 0.160
	K422A	0.0840 ± 0.0170	0.0310 ± 0.0020	0.370 ± 0.053

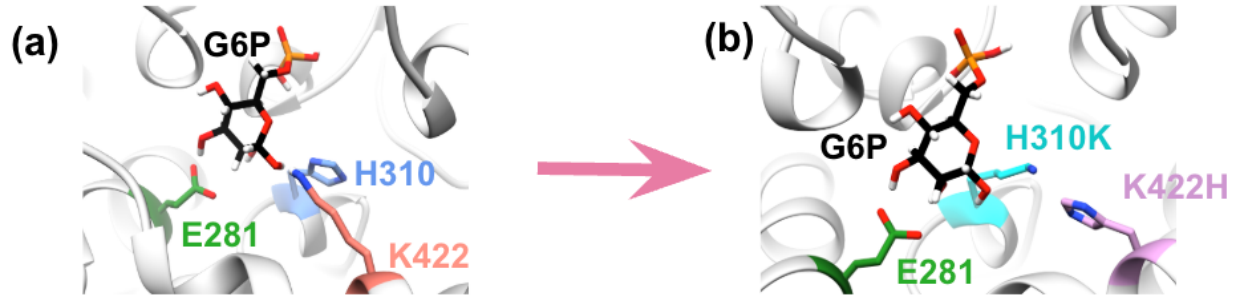

Figure S7. Active site of the WT and K422H/H310K mutant with 422, 310, and E281. Docking was done in Chimera. (a) Active site of the WT TmaPGI with K422/H310 and docked G6P. (b) Active site of proposed double mutant TmaPGI featuring K422H/H310K and docked G6P.

CHEM 4411-105: Andrew Spira

1 May 2025

Honor Pledge: *On my honor as a student, I have neither given nor received unauthorized aid on this assignment.*

Sarah, Madison, Amanda, Alessandra, Sophia, Nicola